Remote Sensing of Environment 134 (2013) 12–23

Contents lists available at SciVerse ScienceDirect

Remote Sensing of Environment

journal homepage: www.elsevier.com/locate/rse

Monitoring meteorological drought in semiarid regions using multi-sensor microwave remote sensing data

Anzhi Zhang, Gensuo Jia *

RCE-TEA, Institute of Atmospheric Physics, Chinese Academy of Sciences, Beijing 100029, China

ARTICLE INFO

Article history:
Received 17 November 2012
Received in revised form 17 January 2013
Accepted 17 February 2013
Available online 21 March 2013

Keywords:
Drought
TRMM precipitation
AMSR-E soil moisture and land surface temperature
Microwave remote sensing
SPI

ABSTRACT

The existing remote sensing drought indices were mainly derived from optical and infrared bands, and have been widely used in monitoring agricultural drought; however, their application in monitoring meteorological drought was limited. This study proposes a new multi-sensor microwave remote sensing drought index, the Microwave Integrated Drought Index (MIDI), for monitoring short-term drought, especially the meteorological drought over semi-arid regions, by integrating three variables: Tropical Rainfall Measuring Mission (TRMM) derived precipitation, Advanced Microwave Scanning Radiometer for EOS (AMSR-E) derived soil moisture, and AMSR-E derived land surface temperature. Each variable was linearly scaled from 0 to 1 for each pixel based on absolute minimum and maximum values over time to relatively monitor drought. Pearson correlation analyses were performed between remote sensing drought indices and scale-dependent Standardized Precipitation Index (SPI) during the growing season (April to October) from 2003 to 2010 to assess the capability of remotely sensed drought indices over three bioclimate regions in northern China. The results showed that MIDI with proper weights of three components outperformed individual remote sensing drought indices and other combined microwave drought indices in monitoring drought. It nearly possessed the best correlations with different time scale SPI; meanwhile it showed the highest correlation with 1-month SPI, and then decreased as SPI time scale increased, suggesting that the MIDI was a very reliable index in monitoring meteorological drought. Furthermore, similar spatial patterns and temporal changes were found between MIDI and 1- or 3-month SPI in monitoring drought. Therefore, the MIDI was recommended to be the optimum drought index, in monitoring short-term drought, especially for meteorological drought over cropland and grassland across northern China or similar regions globally with the ability to work in all weather conditions.

1. Introduction

Drought is the most costly natural disasters in China and all over the world (Huang et al., 2006; Wilhite, 2000). As extreme climate events, droughts are likely to become intensified and more frequent under global warming (Trenberth et al., 2003, 2004), especially in semi-arid regions of the northern hemisphere (Wetherald & Manabe, 1999, 2002). The precipitation of northern China is governed by the East Asian summer monsoon (EASM), the EASM and related seasonal rain belts assume significant variability at intra-seasonal, inter-annual and inter-decadal time scales (Ding, 2007; Ding & Chan, 2005). Furthermore, the EASM has experienced significant weakening since 1970s, thus resulting in increased droughts over northern China (Ding et al., 2008; Wang, 2001), and have adversely affected water resources, agricultural production, and welfare of people across northeastern China, where precipitation limitation is already at high risk (Piao et al., 2010). Clearly, it is very important to monitor drought timely over monsoon frontiers.

Droughts are often considered in four major types: meteorological, agricultural, hydrological, and socioeconomic drought (American Meteorological Society, 1997, 2004; Wilhite, 2005). Meteorological drought results from reduction of precipitation, while agricultural drought is related to shortage of available water for plant growth. Hydrological drought refers to deficiency of surface and subsurface water supply. Finally, socioeconomic drought is associated with insufficient supply to meet the demand of some economic good with the above three types of drought. Meteorological drought occurs more frequently and commonly than other three kinds of droughts; meanwhile, it normally triggers other types of drought, including agricultural, hydrological, and socioeconomic drought (WMO, 2006). Hence, timely meteorological drought monitoring is vitally important for early warning and risk management of water resources and agricultural production.

Drought can be effectively monitored by drought indices derived from station-based meteorological data, such as the percent of

* Corresponding author at: RCE-TEA, Institute of Atmospheric Physics, Chinese Academy of Sciences, PO Box 9804, Beijing 100029, China. Tel.: +86 10 82995314.
E-mail address: jiong@tea.ac.cn (G. Jia).

0034-4257/$ – see front matter © 2013 Elsevier Inc. All rights reserved.
http://dx.doi.org/10.1016/j.rse.2013.02.023

normal precipitation, the Palmer Drought Severity Index (PDSI; Palmer, 1965), Palmer Moisture Anomaly Index (z-index; Palmer, 1965), deciles (Gibbs & Maher, 1967), and the Standardized Precipitation Index (SPI; McKee et al., 1993). Among them, the SPI provides a simple and versatile way to monitor drought with drought categories of near normal (−0.99 to 0.99), moderate drought (−1.49 to −1.0), severe drought (−1.99 to −1.5) and extreme drought (<−2.0) (McKee et al., 1993, 1995). As it is based on statistical probability and is designed to be a spatially invariant indicator of drought, the SPI has improved drought monitoring capabilities and has been accepted broadly by the scientific community (Guttman, 1998; Hayes et al., 1999; Keyantash & Dracup, 2002). The main advantage of the SPI is that it can be flexibly calculated at different temporal scales (e.g., 1-, 3-, 6-, 9-, 12-, and 24-month intervals) according to user's interest for monitoring meteorological, agricultural or hydrological drought (Guttman, 1999).

Station-based drought indices can effectively estimate drought conditions around meteorological station, but the lack of continuous spatial coverage limits the ability of characterizing and monitoring detailed spatial pattern of drought conditions at regional scale, especially in areas with sparse meteorological stations or high degree of spatial variability. Satellite-based remote sensing can overcome the limitations of ground observation; it can consistently and continuously monitor Earth environment processes and changes cross space and time. The detailed space-based observations are natively suitable for regionally oriented phenomena monitoring and detection. Drought indices based on satellite remote sensing data are therefore capable of capturing spatial details and have become the most promising tools for drought monitoring at regional scale (Kogan, 1997).

In recent years, many indices based on remote sensing data have been proposed to monitor drought, such as the Normalized Difference Vegetation Index (NDVI; Rouse et al., 1973), the Vegetation Condition Index (VCI), the Temperature Condition Index (TCI), the Vegetation Heath Index (VHI; Kogan, 1995a,b), the Normalized Difference Water Index (NDWI; Gao, 1996), the Standardized Vegetation Index (SVI; Peters et al., 2002), the Normalized Difference Drought Index (NDDI; Gu et al., 2007), and the Normalized Multiband Drought Index (NMDI; Wang & Qu, 2007). More recently, an integrated remote sensing drought index, the Scaled Drought Condition Index (SDCI), was developed to monitor agricultural drought using multi-sensor data (Rhee et al., 2010).

Most of the current remote sensing drought indices use optical and infrared channels (Table 1) except for SDCI, which consider microwave sensor data. Therefore, those indices are highly related to vegetation condition. Additionally, there is a time lag between precipitation occurrence and vegetation response, and the lag time varies according to several factors, such as the regional rainfall patterns (e.g., Farrar et al., 1994), land cover and vegetation type (e.g., Wan et al., 2004), and soil type (e.g., Ji & Peters, 2003). Therefore, the vegetation related drought indices are more suitable for monitoring agricultural drought (e.g., Quiring & Ganesh, 2010); meanwhile, their applications are largely limited by the atmospheric conditions, especially the clouds. Furthermore, it was found that the assessment capability of drought indices differs greatly between each other in spatial distribution (e.g., Bayarjargal et al., 2006) and varies over time within the growing season (e.g., Karnieli et al., 2010; Vicente-Serrano, 2007) according to their specific observation targets as well as the accuracy and uncertainties from retrieval algorithms. Combination of several drought indices, such as VHI and SDCI, may yield more reliable drought monitoring at region scale. Nevertheless, timely monitoring of short term drought at regional scale, especially meteorological drought, is still a great challenge.

Table 1
Formulas for remote sensing drought indices. ρ represented the spectral reflectance, and α was the weight of single index while constituting the integrated drought indices.

Drought indices	Formula
VCI	$(NDVI_i - NDVI_{min}) / (NDVI_{max} - NDVI_{min})$
TCI	$(T_{max} - T_i) / (T_{max} - T_{min})$
VHI	$\alpha * VCI + (1 - \alpha) * TCI$
NDWI	$(\rho_{NIR} - \rho_{SWIR}) / (\rho_{NIR} + \rho_{SWIR})$
NDDI	(NDVI − NDWI) / (NDVI + NDWI)
NMDI	$(\rho_{NIR} - (\rho_{1640\ nm} - \rho_{2130\ nm})) / (\rho_{NIR} + (\rho_{1640\ nm} - \rho_{2130\ nm}))$
Scaled LST	$(LST_{max} - LST_i) / (LST_{max} - LST_{min})$
Scaled TRMM	$(TRMM_i - TRMM_{min}) / (TRMM_{max} - TRMM_{min})$
Scaled NDVI	$(NDVI_i - NDVI_{min}) / (NDVI_{max} - NDVI_{min})$
SDCI	(1/4) * scaled LST + (2/4) * scaled TRMM + (1/4) * scaled NDVI

To date, the application of microwave remote sensing in drought monitoring has not been thoroughly investigated. In addition to the above remotely sensed drought indices, satellite microwave remote sensing is an important approach for drought monitoring due to its all weather working advantages. It provides abundant variables highly related to various climate parameters, such as precipitation derived from the Tropical Rainfall Measuring Mission (TRMM), land surface temperature (LST) and soil moisture (SM) obtained from the Advanced Microwave Scanning Radiometer (AMSR-E) on-board Aqua satellite. TRMM provides invaluable measurements for quasi-global (50°S–50°N) coverage of rain estimates at 3 hourly or monthly of 0.25° × 0.25° resolution from 1998 (Huffman et al., 2007). The data have been used to effectively monitor precipitation variation and drought (e.g., Jiang & Zipser, 2010; Rhee et al., 2010). Soil moisture is a simple and sensitive index of drought, and was widely used to monitor water deficit (Andreadis et al., 2005; Cai et al., 2009). Observed and simulated soil moisture data were demonstrated as reasonable proxy of PDSI and SPI drought indices (Dai et al., 2004; Sheffield & Wood, 2007). Currently, there are many global soil moisture data sets derived from microwave remote sensing (e.g., De Jeu et al., 2008; Njoku et al., 2003; Wagner et al., 1999), while daily soil moisture derived from AMSR-E may contribute to monitor drought in recent decade from 2002. Land surface temperature derived from thermal infrared data was also widely used to monitor drought (e.g., Karnieli et al., 2010; Rhee et al., 2010). However, LST can be reasonably retrieved from passive microwave techniques independent of clouds, in particular at the Ka band (37 GHz) from satellite sensors (e.g., AMSR-E) (Holmes et al., 2009).

Drought has especially affected the agricultural areas over northern China (Wang et al., 2011). Due to the importance of grassland/cropland in China agricultural production and the practical purpose of meteorological drought monitoring, we especially focused on these two land cover classes. This study aims to develop a multi-sensor microwave remote sensing based drought index (the Microwave Integrated Drought Index; MIDI) by integrating three variables: precipitation, soil moisture, and land surface temperature derived from microwave sensors such as TRMM and AMSR-E, in order to improve timely monitoring of short-term drought especially meteorological drought over semi-arid northern China. Thus, the main objectives of this study are: 1) to assess the capability of microwave drought indices in monitoring drought using SPI as in-situ drought index, by comparing the remote sensing drought indices with different time scale SPI over space and time; 2) to develop microwave integrated multi-sensor drought index for drought monitoring over semi-arid regions; and 3) to investigate the characteristics of microwave multi-sensor remote sensing detected drought maps. The results are expected to improve meteorological drought monitoring approaches by using existing microwave remote sensing data.

2. Study area

Northern China is right on or near the edge of the EASM (Wang & Ho, 2002), and therefore, sensitive to monsoon variability and suffers from frequent droughts. With likely weakening of the EASM, drought in this region is expected to increase. The major land cover categories

of the region were barren or sparely vegetated, grasslands, croplands, mixed forest, and cropland/natural vegetation mosaic, and they accounted for 33%, 27.9%, 18.5%, 6.1%, and 4% of regional land cover respectively as estimated with land cover classifications derived from 2008 MODIS (the Moderate Resolution Imaging Spectroradiometer) data (MCD12Q1).

In order to quantitatively investigate the capability of space-borne microwave precipitation, soil moisture, and land surface temperature in drought monitoring, we selected three subset regions over northern China (Fig. 1): grassland dominated region (A), cropland dominated regions (B) with 1 year 1 harvest, and cropland dominated regions (C) with irrigated area of 1 year 2 harvest or 2 years 3 harvests. The annual mean precipitation was 295, 488, and 687 mm for region A, B, and C respectively. In addition, three subsets were identical in Köppen–Geiger climate classification (Kottek et al., 2006), i.e., BSk (arid steppe with cold arid) accounted for 54.7% of region A; however, Dwa (snow, winter dry with hot summer) and Cwa (warm temperate, winter dry with hot summer) occupied 78.3% and 76.7% of region B and C respectively (Fig. 1 and Table 2).

Table 2
Main characteristics of subset regions over northern China. The Köppen–Geiger climate classification of BSk, Cwa, Dwa, and Dwb refers to arid steppe with cold arid, warm temperate and winter dry with hot summer, snow, winter dry with hot summer, and snow, winter dry with warm summer respectively. The time duration of in-situ precipitation records was from 1960 to 2010.

Region	MODIS IGBP LC		Meteorological data		Köppen–Geiger climate classification	
	Grassland	Cropland	Station number	Annual mean precipitation (mm)		
A	84.2%	8.5%	25	295	BSk (54.7%)	Dwb (27.6%)
B	11.3%	77.8%	24	488	Dwa (78.3%)	Dwb (20.3%)
C	0.3%	78.2%	19	687	Cwa (76.7%)	Dwa (11.6%)

3. Data and methodology

A wide range of meteorological and remote sensing datasets were used to assess multi remote sensing drought indices in monitoring drought over cropland and grassland in northern China for the time period of 2003–2010. The analyses focused on the growing season from April to October when the drought had major impacts.

3.1. In-situ precipitation data and drought indices

Monthly precipitation records of all available stations from 1960 to 2010 were obtained from China meteorological data service (http://data.cma.gov.cn) over the study area. Firstly, the data were aggregated to annual interval, and then interpolated spatially by using Kriging to get average annual precipitation map at 0.5° grid (Fig. 1b). Secondly, the ground precipitation data were used to calculate the in-situ drought indices. Only weather stations located on grassland and croplands within the subset regions with long term data available from 1960 to 2010 were included, thus 25, 24, and 19 weather stations were selected for regions A, B, and C respectively. In this study, the precipitation was assumed to be homogeneous over the corresponding remote sensing pixel (0.25° × 0.25°).

3.1.1. Percent of normal

The percent of normal precipitation (PN) is a simple and effective method to measure precipitation variation for a location. It is calculated as observed precipitation divided by long-term mean precipitation, and multiplied by 100%; while mean precipitation (average of precipitation from 1960 to 2010) is considered to be 100% for a weather station. Percent of normal can be obtained at various time scales from daily to annual. In this study we calculated percent of normal using monthly precipitation data for weather stations over subset regions. The monthly PN for weather stations within each region were averaged to estimate the regional precipitation deficit or meteorological drought condition.

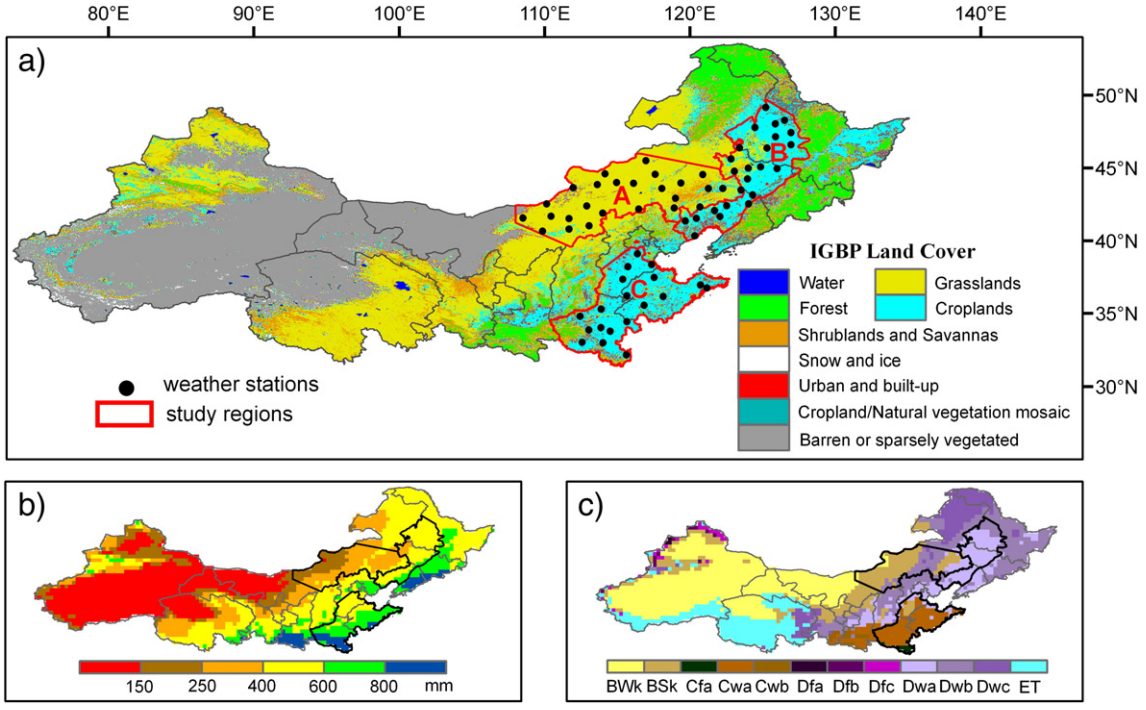

Fig. 1. Study area and climate characteristics. (a) Locations of three subset regions (red polygons) and weather stations (black dots) based on MODIS International Geosphere–Biosphere Program (IGBP) land cover classification map of 2008 MCDQ1, some land cover classes were aggregated into one category; (b) annual mean precipitation from 1960 to 2010 of in-situ weather station observations; and (c) Köppen–Geiger climate classification map. Region A was grassland dominated area; while region B and C were cropland dominated area with different crop rotations: the former was cultivated for 1 year 1 harvest, and cultivation of the latter was 1 year 2 harvest or 2 years 3 harvests.

3.1.2. Standardized Precipitation Index (SPI)

The SPI, developed by Mckee et al. (1993), was designed to quantify precipitation deficit at multiple time scales. The index requires a long-term precipitation record, which was recommended at least 50 years for drought monitor periods of 1 year or less (Guttman, 1999). Thus the long-term monthly precipitation data from 1960 to 2010 were used to construct SPI series at 1-, 3-, 6-, 9-, and 12-month time scales for each weather station. The 1-month SPI was applied to analyze the meteorological drought (Caccamo et al., 2011), while the seasonal scales of 3-month or 6-month SPI were considered to be more appropriate for measuring agricultural drought condition (Rouault & Richard, 2003). Meteorological drought and agricultural drought were typically recognized as short-term drought (Heim, 2002). The 1-month and 3-month SPI for weather stations within each region were averaged to estimate the regional drought condition. Only the data within the growing season were used in the analysis.

3.2. Remote sensing data and drought indices

3.2.1. MODIS data and VCI

Land cover classifications derived from 2008 MODIS data (MCD12Q1, collection v005) were used to locate the grassland and cropland over the region. The land cover scheme identifies 17 land cover classes defined by the International Geosphere-Biosphere Programme (IGBP) at a spatial resolution of 500 m. In addition, monthly cloud-free NDVI time series from 2003 to 2010 with 0.05° resolution (MOD13C2, collection v005) were also obtained from the Land Processes Distributed Active Archive Center (LP DAAC; https://lpdaac.usgs.gov/). The data were resampled to be spatially consistent with the microwave drought variables of 0.25° resolution using pixel aggregate method. Finally, the data were used to calculate VCI with the formula developed by Kogan (Table 1).

3.2.2. TRMM precipitation

TRMM satellite was launched in November 1997, and since then, several algorithms have been developed to estimate rainfall (e.g., Iguchi et al., 2000). In this study, the TRMM Multi-satellite Precipitation Analysis (TMPA) monthly gridded precipitation product was used to monitor precipitation variation and drought (Huffman et al., 2007). The 3B43 dataset was estimated from multiple satellites, as well as gage analyses wherever feasible. It covers the latitude band extends from 50° south to 50° north with 0.25° × 0.25° spatial resolution from 1998 to present, and is given as monthly precipitation rate (mm/h). The dataset from 2003 to 2010 were obtained from the National Aeronautics and Space Administration (NASA) Data and Information Services Center (DISC) (http://mirador.gsfc.nasa.gov/).

3.2.3. AMSR-E soil moisture and land surface temperature

The soil moisture and land surface temperature datasets used in the study were derived with the Land Parameter Retrieval Model (LPRM) jointly developed by the Vrije Universiteit Amsterdam and NASA Goddard Space Flight Center (VUA-NASA) from the descending mode of AMSR-E on board of the AQUA satellite (Holmes et al., 2009; Owe et al., 2008), which was launched in May 2002. The AMSR-E instrument measures radiation at six frequencies in the range of 6.9–89 GHz, all dual polarized, providing near-global coverage every two days or less. The Aqua orbit is sun-synchronous with equator crossings at 1:30 P.M. and 1:30 A.M. local solar time (Njoku et al., 2003). The soil moisture product was L3A in terms of the Atmospheric Data Access for the Geospatial User Community (ADAGUC) standards, which retrieval from 6.9 GHz and 10.7 GHz combined according to the radio frequency interference (RFI) map, applied basic masking and 0.25° grid (Owe et al., 2008). The land surface temperature was obtained from the 37 GHz vertical polarized brightness temperature at 0.25° resolution (Holmes et al., 2009). Intensified validation activities of the VUA-NASA SM/LST datasets were carried out over several regions (e.g., De Jeu et al., 2008; Draper et al., 2009; Parinussa et al., 2008), including northern China (Zhang et al., 2011a,b). These studies found that the VUA-NASA products agreed well with in-situ SM/LST measurements and had a strong correspondence to precipitation in time and space. Therefore, the datasets were aggregated to monthly interval and used here for development of drought indices.

3.3. Microwave remote sensing drought indices

In order to detect and monitor drought timely at regional scale, we propose the TRMM Precipitation Condition Index (PCI), the Soil Moisture Condition Index (SMCI) and the Temperature Condition Index (TCI) based on microwave remote sensed TRMM precipitation, AMSR-E soil moisture and land surface temperature retrievals from 2003 to 2010 (Table 3). The remotely sensed variables were linearly scaled from 0 to 1 for each pixel based on absolute minimum and maximum values for each variable over time, in order to discriminate the weather-related component from the ecosystem component as done for VCI using NDVI (Kogan, 1995a,b). After normalization, the scaled value changed from 0 to 1, corresponding to the precipitation changes from extremely low to optimal.

The microwave remotely sensed variables are derived from low frequency microwave remote sensing, therefore, can work in all weather condition with high temporal resolution (daily product for VUA-NASA AMSR-E SM/LST and 3-hour precipitation product of TRMM 3B42). Consequently, the drought indices can be calculated for multiple time scales (e.g. day, week, half-month, month, season, and year). In this study, the monthly drought indices were calculated for drought monitoring and assessment.

Combinations of the above three microwave remotely sensed drought indices were also tested. The Microwave Integrated Drought Index (MIDI) was an integration of all three components with flexible weights. Additionally, the TRMM Precipitation and Soil Moisture Condition Index (PSMCI), the TRMM Precipitation and Temperature Condition Index (PTCI), and the Soil Moisture and Temperature Condition Index (SMTCI) were integrated by each two components of PCI, SMCI, and TCI with changeable weights respectively (Table 3). All the indices were further assessed with different time scales in-situ SPI for each region.

3.4. Remote sensing drought indices and SPI data analyses

3.4.1. Correlation analyses

Pearson correlation analyses were performed between the remotely sensed drought index values and 1-, 3-, 6-, 9-, and 12-month SPI (SPIs)

Table 3
Descriptions of remote sensing drought indices. α and β represented the weight of single index while constituting the integrated drought indices. The full names and abbreviations of drought indices were as follows: TRMM Precipitation Condition Index (PCI); Soil Moisture Condition Index (SMCI); Temperature (Land Surface Temperature) Condition Index (TCI); Vegetation Condition Index (VCI); TRMM Precipitation and Soil Moisture Condition Index (PSMCI); TRMM Precipitation and Temperature Condition Index (PTCI); Soil Moisture and Temperature Condition Index (SMTCI); and Microwave Integrated Drought Index (MIDI).

Drought Indices	Formula
PCI	$(TRMM_i - TRMM_{min}) / (TRMM_{max} - TRMM_{min})$
SMCI	$(SM_i - SM_{min}) / (SM_{max} - SM_{min})$
TCI	$(LST_{max} - LST_i) / (LST_{max} - LST_{min})$
VCI	$(NDVI_i - NDVI_{min}) / (NDVI_{max} - NDVI_{min})$
PSMCI	$\alpha * PCI + (1 - \alpha) * SMCI$
PTCI	$\alpha * PCI + (1 - \alpha) * TCI$
SMTCI	$\alpha * SMCI + (1 - \alpha) * TCI$
MIDI	$\alpha * PCI + \beta * SMCI + (1 - \alpha - \beta)TCI$

values over each region over growing season from 2003 to 2010 to assess the capability of remotely sensed drought indices in monitoring drought over time and space. Since the relationship between remotely sensed drought indices and SPI varies over time (e.g., Ji & Peters, 2003), we analyzed the correlations for the 7-month growing season from April to October and each month separately. The correlation coefficient and their *p*-value were obtained for each analysis. The remotely sensed index values were extracted according to the in-situ meteorological station location. In order to have the same number of samples for comparison between the remotely sensed drought indices and the in-situ drought index, data were excluded if any index values were unavailable for weather stations during the chosen time period.

3.4.2. Spatial comparisons between the remotely sensed drought maps

A series of maps were created to compare spatial patterns of drought over the region. Maps of multi-year mean precipitation, NDVI, SM, and LST from 2003 to 2010 were created to characterize spatial distribution of remotely sensed variables for July, when yearly peak precipitation occurred over the study region. Meanwhile, drought maps derived from PCI, SMCI, TCI, and VCI in 2010 were spatially analyzed to test their spatial consistency.

3.4.3. MIDI drought maps and comparison with the in-situ drought indices

MIDI drought maps together with 1-month SPI from April to October of 2010 and individual month of July from 2003 to 2010 were developed to depict the seasonal changes and inter-annual variations. Additionally, the drought area derived by the selected MIDI from April to October in 2010 was extracted and compared with that detected by in-situ 1-month SPI (station number under drought divided weather number of each region) for each region separately. The regional averaged and station located pixel averaged MIDI values for July were calculated to investigate the differences within each region. Furthermore, in order to assess the discrepancy of drought indices in monitoring drought for each region, the station located pixels averaged values of another two combined microwave drought indices as well as the above two calculated MIDI values were compared to averaged in-situ percent of normal, 1-month, and 3-month SPI.

4. Results and discussion

4.1. Correlations between remote sensing drought indices and SPI

The correlation coefficients were calculated between remote sensing drought indices and SPIs over three subset regions for the growing season (Table 4). Overall, the correlations varied among regions and different time scales, and were statistically significant at the 0.01 level of significance except for SMCI vs. 12-month SPI as well as VCI vs. 1- and 12-month SPI in cropland dominated region C.

PCI showed the highest correlation with 1-month SPI (*r* around 0.70) when compared to remote sensing drought indices or different time scale SPI; meanwhile, the correlation coefficient decreased as the SPI time scale increased in all three regions (Table 4). This index PCI was most sensitive in monitoring short-term drought especially for meteorological drought. Additionally, the PCI presented the highest correlation with 1-, 3-, 6-, and 9-month SPI compared to remote sensing drought indices in region C (Table 4c), suggesting that the PCI provided more reliable information than other remote sensing drought indices in monitoring drought over this region.

Correlations between SMCI and SPI exhibited different trends in three regions, the *r* values decreased from 0.60 to 0.37 as SPI time scale increased in region A (Table 4a), meanwhile it showed similar trend in region C (Table 4c); in contrast, the 6-month SPI had the highest correlation coefficient with SMCI in region B (Table 4b); suggesting that the SMCI provided valuable information in monitoring

Table 4
Correlations between remote sensing drought indices and in-situ different time scales SPI among three subset regions. The highest *r* values for each row/column in three regions were shown in italics/bold. *p*-value < 0.01 except for data with asterisk (*). Descriptions of drought indices were provided in Table 2. SPI-1 = 1-month SPI; SPI-3 = 3-month SPI; SPI-6 = 6-month SPI; SPI-9 = 9-month SPI; and SPI-12 = 12-month SPI.

Remote sensing index	SPI-1	SPI-3	SPI-6	SPI-9	SPI-12
	r				
a) Region A					
PCI (n = 1400)	**0.71**	0.50	0.49	0.41	0.33
SMCI (n = 1397)	*0.60*	**0.55**	**0.55**	0.47	0.37
TCI (n = 1400)	*0.29*	0.25	0.24	0.23	0.18
VCI (n = 1400)	0.31	0.49	0.48	**0.52**	**0.50**
b) Region B					
PCI (n = 1344)	**0.67**	0.46	0.43	0.37	0.25
SMCI (n = 1326)	0.46	**0.50**	**0.54**	**0.48**	**0.37**
TCI (n = 1344)	*0.41*	0.37	0.32	0.32	0.31
VCI (n = 1344)	0.10	0.23	0.25	*0.26*	0.18
c) Region C					
PCI (n = 1050)	**0.70**	**0.40**	**0.35**	**0.29**	0.20
SMCI (n = 990)	*0.25*	0.23	0.19	0.11	*0.06
TCI (n = 1050)	0.29	*0.33*	*0.33*	**0.29**	**0.24**
VCI (n = 1050)	*0.07	*0.12*	*0.12*	*0.12*	*0.08

meteorological and agricultural droughts for all three regions. Furthermore, SMCI performed the highest correlation with 3- and 6-month SPI in region A and with 3-, 6-, 9-, and 12-month SPI in region B among all available remote sensing drought indices (Table 4a and b).

TCI had the highest correlation coefficient with 1-month SPI, and then the values decreased as time scale increased in regions A and B; moreover, the values were lower than that of PCI and SMCI with SPI (Table 4a and b). However, TCI exhibited stronger correlations with 3- and 6-month SPI than other time scale SPI in region C, and had the highest correlation with 9- and 12-month SPI comparing within remote sensing drought indices (Table 4c).

VCI showed the highest correlation with 9-month SPI in regions A and B (Table 4a and b), as well as 3-, 6-, and 9-month SPI in region C (Table 4c), and the *r* values tended to decrease toward the longer and shorter time scales; hence, the VCI appeared to be less sensitive to short-term precipitation deficiencies, and previous studies showed similar results (e.g., Ji & Peters, 2003). Moreover, the correlations between VCI and 9- and 12-month SPI were the highest compared to microwave drought indices in region A (Table 4a), but it did not perform well in regions B and C (Table 4b and c).

The PCI, SMCI, and VCI generally showed a similar trend in correlation with SPI among precipitation gradient, they had the highest correlations in dry areas (region A with annual precipitation of 295 mm; Table 4a), and the correlations declined in moderate precipitation area (region B with annual precipitation of 488 mm; Table 4b), with the lowest correlation in wetter area (region C with precipitation of 687 mm/year; Table 4c). Generally, TCI presented stronger correlation with SPI in region B over regions A and C. The trend between VCI and SPI in northern China agreed with previous studies carried out in other regions, i.e., the correlations between VCI and SPI were generally higher (lower) in drier (wetter) locations (e.g., Quiring & Ganesh, 2010; Vicente-Serrano, 2007). Here we demonstrated that the microwave remote sensing drought indices may be used to better monitor drought than VCI especially for short-term drought in the study region.

4.2. Temporal correlation between remote sensing drought indices and SPI

Correlation coefficients between remote sensing drought indices and in-situ SPIs for each month during the growing season were summarized (Fig. 2). It could be noted that the *r* values varied greatly by

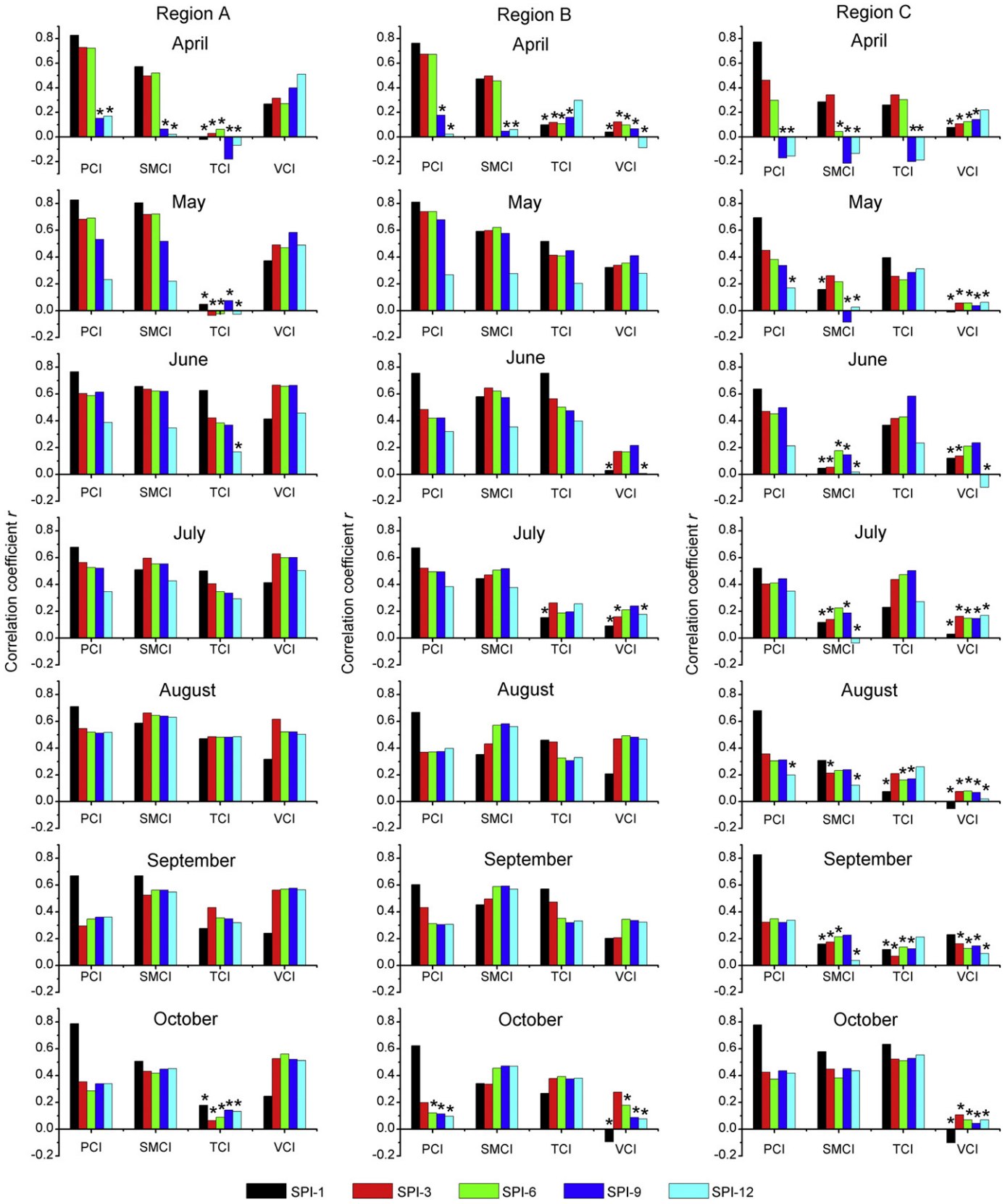

Fig. 2. Correlations between remote sensing drought indices and in-situ different time scales SPI among three subset regions from April to October. *p*-value < 0.01 except for columns with asterisk (*). Descriptions of drought indices were provided in Table 2. SPI-1 = 1-month SPI; SPI-3 = 3-month SPI; SPI-6 = 6-month SPI; SPI-9 = 9-month SPI; and SPI-12 = 12-month SPI.

month and SPI time scale among regions, indicating that the capability of indices in monitoring drought differed greatly along seasonal time.

In the grassland dominated region, remote sensing drought indices were statistically significant at 0.01 level with some exceptions, e.g., TCI vs. all time scale SPI in April, May, and October (left panel

in Fig. 2). In general, PCI was favorable in monitoring 1-month drought, while SMCI and VCI had higher correlations with 3-, 6-, 9-, and 12-month SPI compared to PCI, providing possibilities of integrating different indices for monitoring drought at different time scales. PCI presented the highest positive correlation with 1-month SPI when compared against SMCI, TCI, VCI, or different time scale SPI, and then the *r* values decreased as the time scale increased; such patterns were also found in regions B and C. SMCI had higher *r* values with 1-month SPI at the beginning (April, May, and June) and the end of growing season (September and October) than other time scale SPI, when 3-month SPI were better correlated with SMCI in July and August. It was indicated that PCI and SMCI were suitable for monitoring short-term drought in such area, while VCI was always correlated to longer time scale SPI. The 3-month SPI showed the highest correlation in summer time, whereas longer time scale SPI were largely correlated with VCI during spring and autumn, these may indicate that vegetation in this area was more sensitive to precipitation during summer time, consequently vegetation was susceptible to precipitation deficiency during the high biomass period. Although the correlations between TCI and SPI were weaker than PCI, SMCI, and VCI compared against SPI, it could also provide valuable information especially in monitoring drought occurring from June to September.

Correlations between SMCI and SPI showed higher values with longer time scale SPI, e.g. with 6-month SPI in May, and 9-month SPI from July to October in region B; meanwhile, the correlations with 3-, 6-, 9-, and 12-month SPI were nearly the highest compared to PCI, VCI, and TCI, suggesting that it was more appropriate for monitoring agricultural or hydrological drought (Fig. 2). TCI was not significantly correlated to 1-month SPI in April and May as well as 3-, 6-, and 9-month SPI in April ($p > 0.01$); however, it had greater correlations with 1-month SPI during 57% of the growing season, likely indicating that TCI was sensitive to short-term precipitation variation. VCI had lower correlations with SPI in region B than region A, in addition, the low correlations in April, June, July, and October demonstrated that less information was provided by SPI in detecting vegetation water stress.

In general, PCI, SMCI, and VCI showed the lowest correlation with SPI in region C compared to that in regions A and B. Two aspects may explain the reason why the lowest correlation of SMCI occurred in

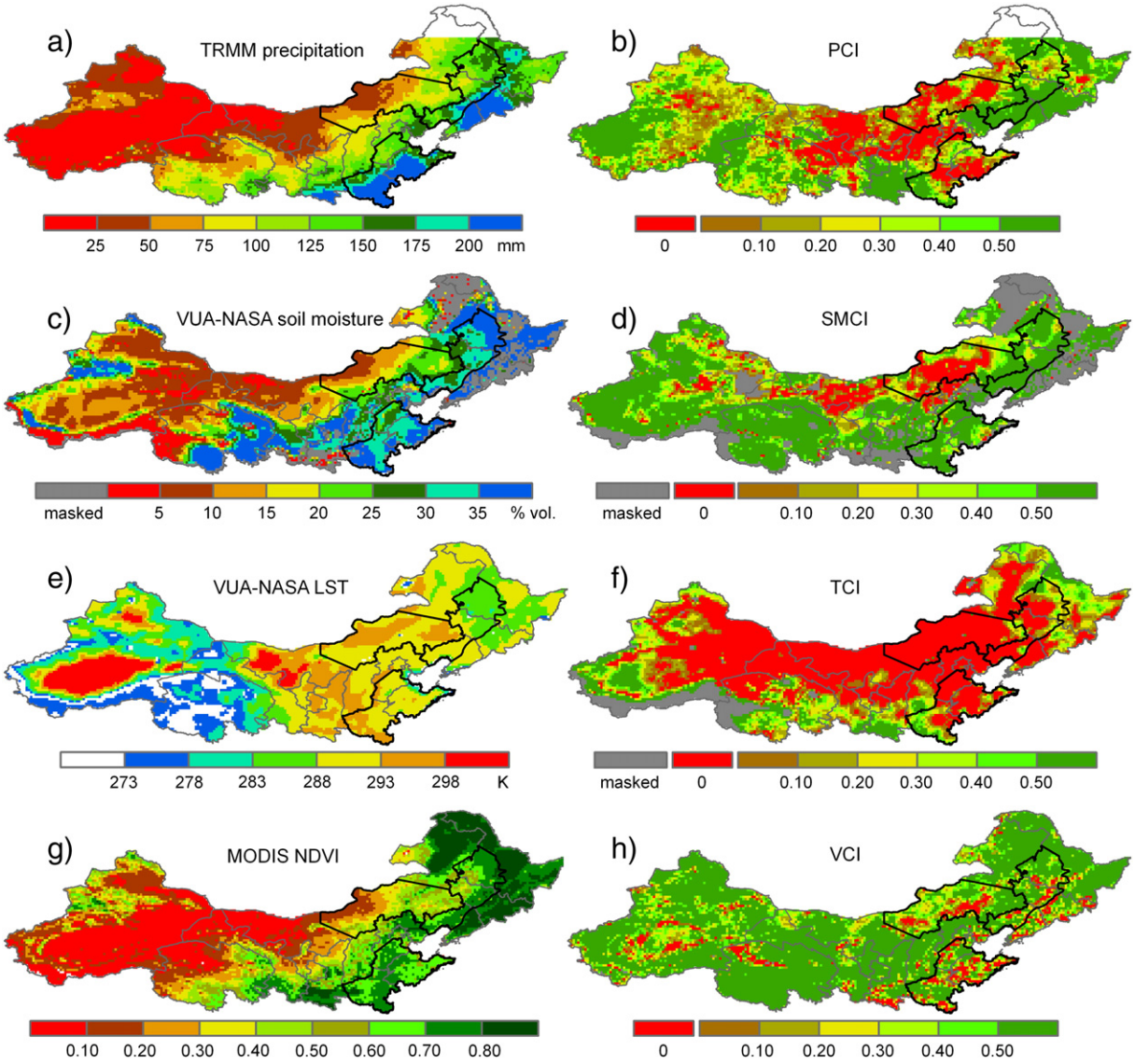

Fig. 3. Drought detected by remote sensing indices for July of 2010 over northern China. For (a), (c), (e), and (g) were 2003–2010 mean TRMM precipitation, VUA-NASA soil moisture, VUA-NASA land surface temperature, and MODIS NDVI for July; while (b), (d), (f), and (h) were drought detected by PCI, SMCI, TCI, and VCI for July of 2010 respectively. Soil moisture and SMCI of forest were masked out in (c) and (d), while areas of SMCI/TCI in (d)/(f) corresponding to zero soil moisture/land surface temperature in July of 2010 were masked out too. Descriptions of drought indices were provided in Table 2.

region C. Firstly, the VUA-NASA passive microwave derived soil moisture showed good agreement with in-situ observations over areas of low vegetation to moderate density, but performance declined with vegetation density increased (e.g., Liu et al., 2012; Owe et al., 2008). In July, NDVI increased from regions A to B and C, therefore resulting in decreased agreement with ground measurements, that were consistent with correlations declining trend from regions A to B and C (Fig. 3g). Secondly, soil moisture variations were not only influenced by precipitation, but also regulated by other factors such as irrigation, thus the accordance between variation of precipitation and soil moisture was reduced in region C, inducing lower correlation between SMCI and SPI while the latter only accounted for precipitation variation (McKee et al., 1993, 1995). In comparison, TCI presented better correlation with SPI than SMCI and VCI in region C. VCI was not significantly correlated to SPI nearly during the whole growing season; this may be partly due to intensive human management in cropland, e.g., irrigation, fertilization, crop rotations, resulted in human-induced variations from year to year, and reduced correlation between vegetation growth and precipitation (SPI only consider precipitation). These results are supported by previous findings, i.e., wetter climate, irrigation, and crop rotations would reduce the strength of correlation between VCI and in-situ drought index (e.g., Piao et al., 2003; Vicente-Serrano, 2007).

4.3. Spatial comparisons of remote sensing drought maps

A series of maps were created to compare spatial patterns of remotely sensed drought (Fig. 3). Satellite derived variables of multi-year mean precipitation (Fig. 3a), soil moisture (Fig. 3c), and NDVI (Fig. 3g) for July provided strong spatial correspondences with annual mean precipitation (Fig. 1b), they all gradually declined from southeast to northwest, which was especially obvious in region A; indicating that remotely sensed variables were largely associated with precipitation, and could be used to detect precipitation variation and drought induced by precipitation declining.

The spatial patterns detected by drought indices differed greatly from each other; and areas with spatial coincidence between them were relatively small. Drought detected by TCI was the largest and severest, followed by PCI and SMCI, while VCI possessed the smallest drought affected area according to the same thresholds for drought severity classification (Fig. 3b,d,f, and h). Disagreements of spatial extent between several remotely sensed drought indices were also found by using change vector analyses (CVA) conducted in adjacent Mongolia (Bayarjargal et al., 2006). The disagreement may be due to the remote sensing variable's specific observation targets as well as the accuracy and uncertainties from retrieval algorithms; taken PCI and VCI for instance, the former only indicates current precipitation, while the latter is not only affected by precipitation, but also influenced by land use factors, such as pest, disease, nutrient input, and grazing (Ji & Peters, 2003). In addition the strength of correlations with in-situ drought indices SPI may also have induced the disagreement of drought detected by remote sensing variables. The disagreement revealed the uncertainty and reliability of remotely sensed indices in assessing droughts, and suggested that the applications of individual indices in drought monitoring should be treated with caution. Combination of different remotely sensed indices may be a reasonable approach for better monitoring regional drought events.

4.4. Optimal microwave integrated drought indices

The microwave drought indices basically performed better than VCI in correlation with in-situ drought index for each month and entire growing season especially in cropland dominated regions (Table 4 and Fig. 2); therefore integrated microwave drought indices with different weights were proposed in development of satellite based drought monitoring platform. Meanwhile, in order to be comparable in time during the growing season and maintain the continuity in space over different regions, the assessments were conducted for the entire growing season across the regions (Table 5). All the correlations were statistically significant ($p < 0.01$). The integrated drought indices showed the highest correlation with 1-month SPI in all subset regions, while the correlation coefficient values declined as the SPI time scale increased (Table 5). This suggests that those drought indices were especially suitable for monitoring meteorological drought. This was an important complementarity to the existing

Table 5
Correlation coefficient *r* values between integrated remote sensing drought indices and in-situ different time scales SPI among three subset regions ($p < 0.01$). The highest *r* values of each integrated drought index for each row/column in three regions were shown in italics/bold. Descriptions of drought indices were provided in Table 2. SPI-1 = 1-month SPI; SPI-3 = 3-month SPI; SPI-6 = 6-month SPI; SPI-9 = 9-month SPI; and SPI-12 = 12-month SPI.

r																			
Indices	Weight			a) Region A (n = 1397)					b) Region B (n = 1326)					c) Region C (n = 990)					
	PCI	SMCI	TCI	SPI-1	SPI-3	SPI-6	SPI-9	SPI-12	SPI-1	SPI-3	SPI-6	SPI-9	SPI-12	SPI-1	SPI-3	SPI-6	SPI-9	SPI-12
PSMCI	0.3	0.7		*0.69*	**0.58**	**0.58**	**0.50**	**0.39**	*0.60*	0.56	**0.59**	**0.52**	**0.39**	*0.47*	0.34	0.29	0.20	0.12
	0.4	0.6		*0.71*	**0.58**	**0.58**	**0.50**	**0.39**	*0.64*	**0.57**	**0.59**	**0.52**	0.38	*0.55*	0.38	0.32	0.23	0.14
	0.5	0.5		*0.72*	**0.58**	**0.58**	0.49	**0.39**	*0.67*	**0.57**	0.58	0.51	0.37	*0.61*	0.41	0.35	0.25	0.16
	0.6	0.4		*0.73*	0.57	0.57	0.48	0.38	*0.69*	0.56	0.56	0.49	0.35	*0.66*	0.42	0.36	0.27	0.18
	0.7	0.3		**0.74**	0.56	0.55	0.47	0.37	**0.70**	0.55	0.54	0.47	0.33	**0.70**	**0.43**	**0.37**	**0.28**	**0.19**
PTCI	0.3		0.7	*0.51*	0.40	0.38	0.35	0.27	*0.57*	0.47	0.42	0.39	**0.34**	*0.51*	0.44	0.41	0.36	**0.29**
	0.4		0.6	*0.58*	0.44	0.43	0.39	0.30	*0.62*	0.49	0.45	0.41	**0.34**	*0.57*	0.46	0.42	**0.37**	**0.29**
	0.5		0.5	*0.64*	0.48	0.46	0.41	0.33	*0.65*	**0.51**	0.46	**0.42**	**0.34**	*0.63*	**0.47**	**0.43**	**0.37**	0.28
	0.6		0.4	*0.68*	0.50	0.49	0.43	0.34	*0.68*	**0.51**	**0.47**	**0.42**	0.33	*0.67*	**0.47**	0.42	0.36	0.27
	0.7		0.3	**0.71**	**0.51**	**0.50**	**0.44**	**0.35**	**0.69**	**0.51**	**0.47**	**0.42**	0.31	**0.70**	0.46	0.41	0.35	0.26
SMTCI		0.3	0.7	*0.45*	0.40	0.39	0.36	0.28	*0.51*	0.49	0.47	0.44	0.40	*0.37*	**0.40**	**0.38**	**0.32**	**0.25**
		0.4	0.6	*0.50*	0.45	0.44	0.40	0.31	*0.53*	0.52	0.51	0.48	0.42	**0.38**	**0.40**	**0.38**	0.31	0.24
		0.5	0.5	*0.54*	0.49	0.48	0.43	0.34	**0.55**	0.54	0.55	0.50	**0.43**	**0.38**	0.39	0.36	0.28	0.21
		0.6	0.4	*0.57*	0.52	0.52	0.45	0.36	*0.54*	**0.55**	**0.57**	**0.52**	**0.43**	*0.36*	0.36	0.34	0.25	0.18
		0.7	0.3	**0.59**	**0.54**	**0.54**	**0.47**	**0.37**	*0.53*	**0.55**	**0.57**	**0.52**	**0.43**	*0.34*	0.33	0.30	0.21	0.15
MIDI	0.3	0.4	0.3	*0.69*	0.57	0.56	0.49	0.38	*0.67*	**0.60**	0.59	0.53	**0.42**	*0.59*	0.46	0.42	0.32	0.23
	0.3	0.5	0.2	*0.70*	0.58	**0.58**	**0.50**	0.39	*0.66*	0.59	**0.60**	**0.54**	**0.42**	*0.56*	0.43	0.38	0.28	0.20
	0.4	0.3	0.3	*0.70*	0.56	0.56	0.48	0.38	*0.70*	0.59	0.57	0.51	0.40	*0.65*	**0.48**	**0.43**	**0.35**	**0.25**
	0.4	0.4	0.2	*0.72*	0.58	0.57	**0.50**	0.39	*0.69*	0.59	0.59	0.53	0.40	*0.63*	0.46	0.41	0.31	0.22
	0.4	0.5	0.1	*0.72*	**0.59**	**0.58**	**0.50**	**0.40**	*0.67*	0.59	**0.60**	0.53	0.39	*0.60*	0.42	0.37	0.27	0.18
	0.5	0.3	0.2	**0.73**	0.57	0.57	0.49	0.39	**0.71**	0.58	0.57	0.50	0.38	**0.68**	0.47	0.42	0.33	0.23
	0.5	0.4	0.1	**0.73**	0.58	**0.58**	0.49	0.39	*0.70*	0.58	0.58	0.51	0.38	*0.66*	0.45	0.39	0.29	0.20

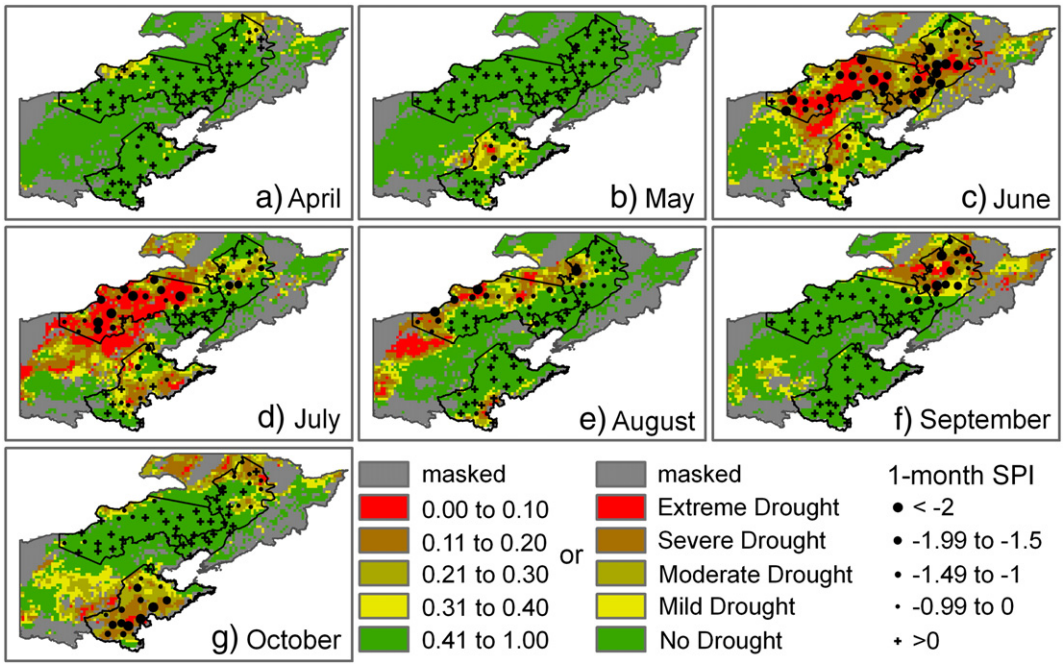

Fig. 4. Seasonal changes of drought detected by MIDI and 1-month SPI from April to October in 2010. Areas with land cover types of forest and barren or sparely vegetated were masked out.

remote sensing drought indices, while they were more related to agricultural or hydrological drought (e.g., Caccamo et al., 2011).

Among integrated drought indices, the PSMCI performed better in regions A and B than PTCI and SMTCI. However, the PTCI showed higher correlations with SPI in region C than other two integrated indices. The *r* values between PSMCI and 1-month SPI increased as the weight of PCI increased in all subset regions. While the correlations between PSMCI and SPIs improved as the weight of PCI increased in region C (Table 5c); in contrast, correlations with longer time scales showed opposite trend in regions A and B (Table 5a and b). The PTCI with larger weight of PCI yielded higher correlations with SPIs in regions A and B except for 12-month SPI in region B (Table 5a and b). However, the *r*-value was the highest between PTCI and 3-, 6-, and 9-month SPI when PCI and TCI had an equal weight of 0.5; meanwhile, the correlations showed opposite trend with 1-month and 12-month SPI as the weights changed (Table 5c). It demonstrated that users could flexibly select the weights for drought monitoring according to their own purpose.

Additionally, PSMCI and PTCI with proper weights performed better correlation than the best individual microwave drought indices with SPIs in the study area; e. g., PSMCI with PCI weight of 0.5 in regions A and B, so as PTCI with PCI weight of 0.7 in region C. These

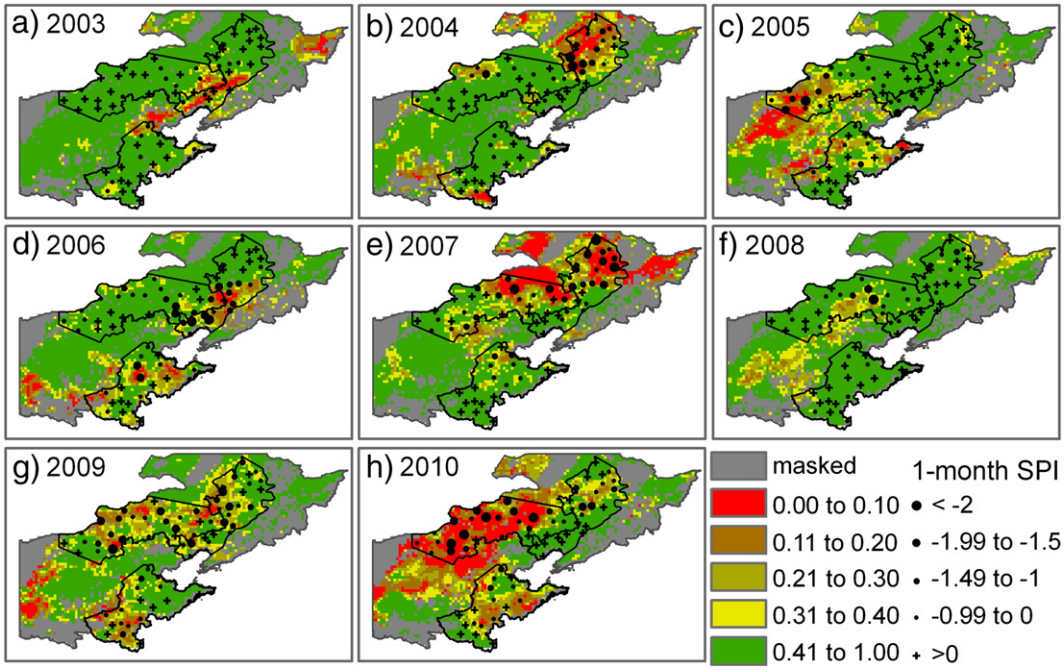

Fig. 5. Year-to-year maps of MIDI and 1-month SPI for July from 2003 to 2010. Areas with land cover types of forest and barren or sparely vegetated were masked out.

results implied that combined unitization of the individual microwave remotely sensed drought indices enhanced the relationships with in-situ drought indices, while similar results have been found in other studies (e.g., Rhee et al., 2010).

Several sets of weights were tested for Microwave Integrated Drought Index (MIDI) against various time scales of SPI over subset regions (Table 5). The MIDI showed the highest correlations with 1-month SPI in all cases; additionally, the correlations generally decreased as SPI time scale increased, meanwhile the *r* values were similar or better than that of PSMCI with proper weights in regions A and B, as well as PTCI in region C. Therefore, MIDI was proposed as an optimum microwave remote sensing drought index that outperformed PSMCI and PTCI in monitoring drought over the region. Among the various sets of weights, according to the relatively higher correlations with different time scale SPI over all three regions, the MIDI with weights of 0.5, 0.3, and 0.2 for PCI, SMCI, and TCI respectively were recommended as reliable microwave remote sensing drought index in monitoring short-term drought, especially for meteorological drought, over northern China (Table 5). Ideally, the precipitation, soil moisture and land surface temperature datasets used in the MIDI are supposed to be totally independent. In this study, the LST and SM are not entirely independent according to LPRM algorithm (Liu et al., 2010; Owe et al., 2008); further studies using independent datasets of MIDI components derived from different algorithms or sensors are needed and will be included in subsequent studies.

4.5. MIDI drought maps and comparisons with the SPI

Since the main purpose of this study was to find an optimum microwave remote sensing based drought index that could be used especially for meteorological drought monitoring, spatial dataset of MIDI from April to September in 2010 (Fig. 4) and for July 2003–2010 (Fig. 5) were illustrated and compared to 1-month SPI over subset regions. Drought severity of MIDI was arbitrarily classified to four levels for purpose of visually comparing with SPI, which was similar to a combined remote sensing drought index of SDCI (Rhee et al., 2010).

There were some discrepancies between MIDI and 1-month SPI derived drought patterns. For example, in September of 2010, mild to severe drought was detected by SPI in northeastern part of region A, but drought captured by MIDI was less severe (Fig. 4f). In addition the MIDI data showed severe to extreme drought in July of 2003 over southern part of region B, but no drought was detected by 1-month SPI (Fig. 5a). In most cases the two indices basically provided similar spatial pattern and consistent seasonal and inter-annual changes. Severe to extreme drought in region A was revealed by MIDI in July of 2010, with SPI values near −1, indicating moderate to extreme drought in the area (Fig. 4d). In July of 2004, MIDI and SPI provided similar spatial pattern in region B with increased drought severity from east to west (Fig. 5b). The spatial patterns of MIDI in July of 2010 demonstrated its stronger spatial consistent with 1-month SPI as compared to that of PCI, TCI, and SMCI (Figs. 3 and 5h). The strong spatial agreement between MIDI and SPI indicated the potential usage of this microwave drought index for timely drought monitoring over northern China and similar regions globally.

Changes of seasonal drought area were analyzed and compared with MIDI (values below 0.4 were assigned as drought) and 1-month SPI datasets (Fig. 6). Although MIDI presented larger drought area than SPI, they basically followed similar patterns over subset regions. There was an exception in region C, while drought area of MIDI increased from June to July, but the change of SPI was opposite (Fig. 6c), this was possibly due to exceptional TRMM precipitation deficiency and high temperature occurred in region C (Fig. 3b and f).

Temporal variations of space-borne microwave indices were compared against percent of normal, 1-month, and 3-month SPI for July over subset regions (Fig. 7). Value of station and region averaged MIDI was close to each other, and possessed similar temporal

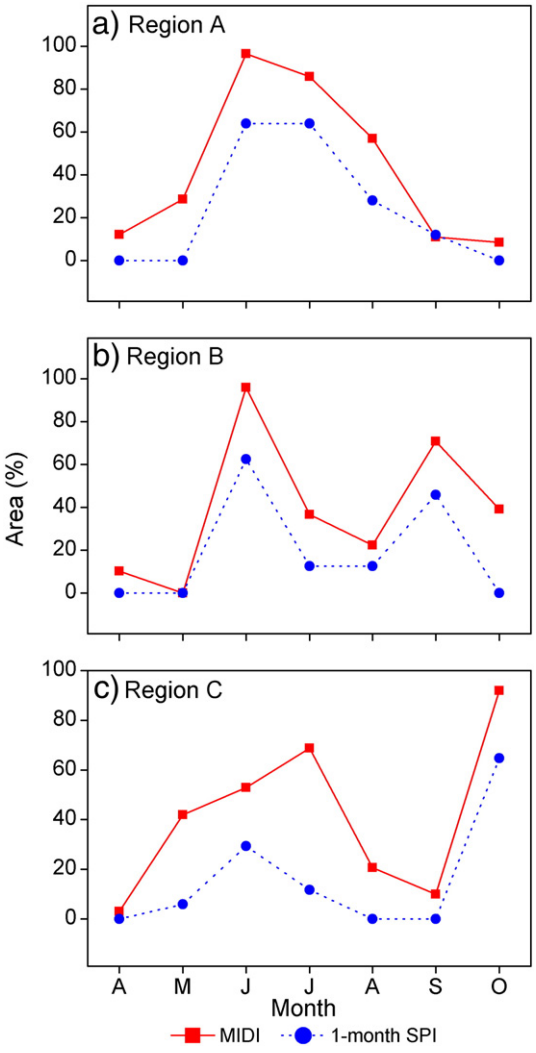

Fig. 6. The drought area identified by MIDI and 1-month SPI for (a) region A, (b) region B, and (c) region C from April to October for 2010.

variations over subset regions, indicating that the station averaged remote sensing drought indices were able to represent the conditions of entire region; therefore reasonable comparability existed between averaged remote sensing and in-situ drought indices. Furthermore, PSMCI (0.6PCI + 0.4SMCI) showed similar temporal variations with MIDI in regions A and B (Fig. 7a and b), so did PTCI (0.6PCI + 0.4TCI) in region C (Fig. 7c), together with results of correlation analyses (Table 5), suggesting that PSMCI and PTCI were comparable with MIDI in monitoring drought over regions A, B, or C respectively.

The percent of normal and 1-month SPI exhibited the similar variations over three regions. The in-situ drought indices basically presented similar changes with microwave remote sensing drought indices. All drought indices showed consistent temporal variation in region B (Fig. 7b), while remote sensing drought indices exhibited different changes compared to 1-month SPI (percent of normal) in 2007 and 3-month SPI in 2010 over region A (Fig. 7a). Meanwhile, 1-month SPI (percent of normal) had better covariation with MIDI, and 3-month SPI agreed better with PTCI in region C (Fig. 7c). Since some discrepancies existed between remote sensing drought indices and in-situ drought indices in term of inter-annual changes, the overall agreement of temporal changes had proven that the MIDI is a reliable integrated index in monitoring meteorological drought (1-month SPI) as well as agricultural drought (3-month SPI) over northern China.

In this study, weights of MIDI in detecting drought were assigned to be the same over northern China. The performances of MIDI might

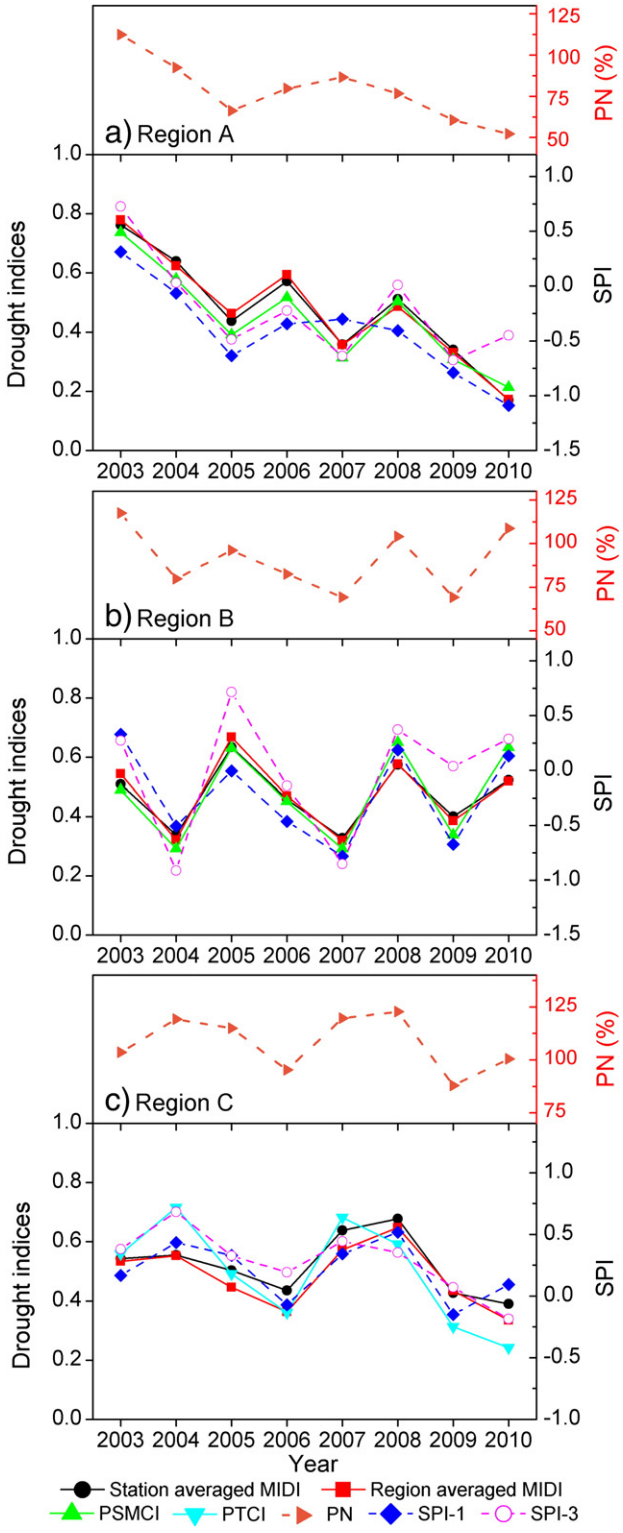

Fig. 7. Year-to-year changes of MIDI, PSMCI, PTCI, percent of normal (PN), and SPI for (a) region A, (b) region B, and (c) region C for July from 2003 to 2010. SPI-1 = 1-month SPI; and SPI-3 = 3-month SPI.

be improved if the weights of three individual microwave indices were adjusted to the optimum according to their performances in each subset region. Furthermore, more meaningful thresholds for MIDI drought severity classification needed to be further studied as more data available with time in further works. The most important finding of this research was a valuable approach to apply microwave satellite remote sensing in short-term drought, especially for meteorological drought monitoring, by using multi-sensor microwave data with the ability to work in all weather conditions.

5. Conclusion

This study assessed the spatial and temporal performances of microwave remote sensing drought indices by comparing them against different time scale SPI over cropland and grassland in northern China during growing season (April to October). Here we demonstrated that the remote sensing drought indices were significantly correlated with field based SPIs in terms of intensity, frequency, and over various land surfaces. We conclude that the microwave remote sensing drought indices performed better for monitoring short-term drought in the study region, while PCI was suitable for monitoring meteorological drought as an individual microwave drought index.

MIDI with proper weights of PCI, SMCI, and TCI was found to be the most reliable microwave index for monitoring droughts over northern China. Meanwhile, it outperformed individual microwave drought indices as well as PSMCI, PTCI, and SMTCI for monitoring drought, as demonstrated by testing several combination weights over study area. Furthermore, similar spatial patterns and temporal changes were found between MIDI and 1- or 3-month SPI over subset regions. In conclusion, MIDI was recommended as an optimum microwave remote sensing index in monitoring short-term drought, especially meteorological drought, for grassland and cropland across northern China or similar regions globally at regional scale with the ability to work in all weather conditions.

Acknowledgments

This study was supported by National Basic Research Program of China (Grant No. 2009CB723904 and 2012CB956202) and National Natural Science Foundation of China (Grant No. 41120114001). We thank ADAGUC for providing AMSR-E derived datasets and algorithms.

Appendix A. Supplementary data

Supplementary data associated with this article can be found in the online version, at http://dx.doi.org/10.1016/j.rse.2013.02.023. These data include Google maps of the most important areas described in this article.

References

American Meteorological Society. (1997). Meteorological drought—Policy statement. *Bulletin of the American Meteorological Society*, *78*, 847–849.
American Meteorological Society. (2004). AMS statement on meteorological drought. *Bulletin of the American Meteorological Society*, *85*, 771–773.
Andreadis, K. M., Clark, E. A., Wood, A. W., Hamlet, A. F., & Lettenmaier, D. P. (2005). Twentieth-century drought in the conterminous United States. *Journal of Hydrometeorology*, *6*, 985–1001.
Bayarjargal, Y., Karnieli, A., Bayasgalan, M., Khudulmur, S., Gandush, C., & Tucker, C. J. (2006). A comparative study of NOAA-AVHRR derived drought indices using change vector analysis. *Remote Sensing of Environment*, *105*, 9–22.
Caccamo, G., Chisholm, L. A., Bradstock, R. A., & Puotinen, M. L. (2011). Assessing the sensitivity of MODIS to monitor drought in high biomass ecosystems. *Remote Sensing of Environment*, *115*, 2626–2639.
Cai, W., Cowan, T., Briggs, P., & Raupach, M. (2009). Rising temperature depletes soil moisture and exacerbates severe drought conditions across southeast Australia. *Geophysical Research Letters*, *36*, L21709. http://dx.doi.org/10.1029/2009GL040334.
Dai, A., Trenberth, K. E., & Qian, T. (2004). A global data set of Palmer Drought Severity Index for 1870–2002: Relationship with soil moisture and effects of surface warming. *Journal of Hydrometeorology*, *5*, 1117–1130.
De Jeu, R. A. M., Wagner, W., Holmes, T. R. H., Dolman, A. J., van de Giesen, N. C., & Friesen, J. (2008). Global soil moisture patterns observed by space borne microwave radiometers and scatterometers. *Surveys in Geophysics*, *29*, 399–420.
Ding, Y. H. (2007). The variability of the Asian summer monsoon. *Journal of the Meteorological Society of Japan*, *85B*, 21–54.
Ding, Y. H., & Chan, C. L. (2005). The East Asian summer monsoon: An overview. *Meteorology and Atmospheric Physics*, *89*, 117–142.
Ding, Y. H., Wang, Z. Y., & Sun, Y. (2008). Inter-decadal variation of the summer precipitation in East China and its association with decreasing Asian summer monsoon. Part I: Observed evidences. *International Journal of Climatology*, *28*, 1139–1161.

Draper, C. S., Walker, J. P., Steinle, P. J., De Jeu, R. A. M., & Holmes, R. H. T. (2009). An evaluation of AMSR-E derived soil moisture over Australia. *Remote Sensing of Environment*, *113*, 703–710.

Farrar, T. J., Nicholson, S. E., & Lare, A. R. (1994). The influence of soil type on the relationships between NDVI, rainfall, and soil moisture in semiarid Botswana: II. NDVI response to soil. *Remote Sensing of Environment*, *50*, 121–133.

Gao, B. (1996). NDWI—A normalized difference water index for remote sensing of vegetation liquid water from space. *Remote Sensing of Environment*, *58*, 257–266.

Gibbs, W. J., & Maher, J. V. (1967). Rainfall deciles as drought indicators. *Australian Bureau of Meteorology Bulletin*, *48* (37 pp.).

Gu, Y., Brown, J. F., Verdin, J. P., & Wardlow, B. (2007). A five-year analysis of MODIS NDVI and NDWI for grassland drought assessment over the central Great Plains of the United States. *Geophysical Research Letters*, *34*, L06407. http://dx.doi.org/10.1029/2006GL029127.

Guttman, N. B. (1998). Comparing the Palmer drought index and the standardized precipitation index. *Journal of the American Water Resources Association*, *34*, 113–121.

Guttman, N. B. (1999). Accepting the standardized precipitation index: A calculation algorithm. *Journal of the American Water Resources Association*, *35*, 311–322.

Hayes, M. J., Svoboda, M. D., Wilhite, D. A., & Vanyarkho, O. V. (1999). Monitoring the 1996 drought using the standardized precipitation index. *Bulletin of the American Meteorological Society*, *80*, 429–438.

Heim, R. R., Jr. (2002). A review of twentieth century drought indices used in the United States. *Bulletin of the American Meteorological Society*, *83*, 1149–1165.

Holmes, T. R. H., De Jeu, R. A. M., Owe, M., & Dolman, A. J. (2009). Land surface temperature from Ka band (37 GHz) passive microwave observations. *Journal of Geophysical Research*, *114*, D04113. http://dx.doi.org/10.1029/2008JD010257.

Huang, R. H., Cai, R. S., Chen, J. L., & Zhou, L. T. (2006). Interdecaldal variations of drought and flooding disasters in China and their association with the East Asian Climate System. *Chinese Journal of Atmospheric Sciences*, *30*, 730–743 (in Chinese).

Huffman, G. J., Adler, R. F., Bolvin, D. T., Gu, G. J., Nelkin, E. J., Bowman, K. P., et al. (2007). The TRMM Multisatellite Precipitation Analysis (TMPA): Quasi-global, multiyear, combined-sensor precipitation estimates at fine scales. *Journal of Hydrometeorology*, *8*, 38–55.

Iguchi, T., Kozu, T., Meneghini, R., Awaka, J., & Okamoto, K. (2000). Rain-profiling algorithm for the TRMM precipitation radar. *Journal of Applied Meteorology*, *39*, 2038–2052.

Ji, L., & Peters, A. J. (2003). Assessing vegetation response to drought in the northern Great Plains using vegetation and drought indices. *Remote Sensing of Environment*, *87*, 85–98.

Jiang, H. Y., & Zipser, E. J. (2010). Contribution of tropical cyclones to the global precipitation from eight seasons of TRMM data: Regional, seasonal, and interannual variations. *Journal of Climate*, *23*, 1526–1543.

Karnieli, A., Agam, N., Pinker, R. T., Anderson, M., Imhoff, M. L., Gutman, G. G., et al. (2010). Use of NDVI and land surface temperature for drought assessment: Merits and limitations. *Journal of Climate*, *23*, 618–633.

Keyantash, J., & Dracup, J. A. (2002). The quantification of drought: An evaluation of drought indices. *Bulletin of the American Meteorological Society*, *83*, 1167–1180.

Kogan, F. N. (1995a). Drought of the late 1980s in the United States as derived from NOAA polar-orbiting satellite data. *Bulletin of the American Meteorological Society*, *76*, 655–668.

Kogan, F. N. (1995b). Application of vegetation index and brightness temperature for drought detection. *Advanced Space Research*, *15*, 91–100.

Kogan, F. N. (1997). Global drought watch from space. *Bulletin of the American Meteorological Society*, *78*, 621–636.

Kottek, M., Grieser, J., Beck, C., Rudolf, B., & Rubel, F. (2006). World map of the Köppen–Geiger climate classification updated. *Meteorologische Zeitschrift*, *15*, 259–263.

Liu, Y. Y., Dorigo, W. A., Parinussa, R. M., De Jeu, R. A. M., Wagner, W., McCabe, M. F., et al. (2012). Trend-preserving blending of passive and active microwave soil moisture retrievals. *Remote Sensing of Environment*, *123*, 280–297.

Liu, Y. Y., Evans, J. P., McCabe, M. F., De Jeu, R. A. M., van Dijk, A. I. J. M., & Su, H. (2010). Influence of cracking clays on satellite estimated and model simulated soil moisture. *Hydrology and Earth System Sciences*, *14*, 979–990.

McKee, T. B., Doesken, N. J., & Kliest, J. (1993). The relationship of drought frequency and duration to time scales. *Proceedings of the 8th Conference on Applied Climatology* (pp. 179–184). Anaheim, CA: American Meteorological Society Boston.

McKee, T. B., Doesken, N. J., & Kleist, J. (1995). Drought monitoring with multiple time scales. *Proceedings of the 9th Conference on Applied Climatology* (pp. 233–236). Dallas, TX: American Meteorological Society.

Njoku, E., Jackson, T. J., Lakshmi, V., Chane, T., & Nghiem, S. (2003). Soil moisture retrieval from AMSR-E. *IEEE Transactions on Geoscience and Remote Sensing*, *41*, 215–229.

Owe, M., De Jeu, R. A. M., & Holmes, T. R. H. (2008). Multisensor historical climatology of satellite-derived global land surface moisture. *Journal of Geophysical Research*, *113*, F01002. http://dx.doi.org/10.1029/2007JF000769.

Palmer, W. C. (1965). Meteorological drought. *Research Paper No. 45*. Washington, D.C.: U.S. Department of Commerce Weather Bureau.

Parinussa, R. M., De Jeu, R. A. M., Holmes, T. R. H., & Walker, J. P. (2008). Comparison of Microwave and infrared land surface temperature products over the NAFE'06 research sites. *IEEE Geoscience and Remote Sensing Letters*, *5*, 783–787.

Peters, A. J., Walter-Shea, E. A., Ji, L., Viña, A., Hayes, M., & Svoboda, M. D. (2002). Drought monitoring with NDVI-based standardized vegetation index. *Photogrammetric Engineering and Remote Sensing*, *68*, 71–75.

Piao, S. L., Ciais, P., Huang, Y., Shen, Z. H., Peng, S. S., Li, J. S., et al. (2010). The impacts of climate change on water resources and agriculture in China. *Nature*, *467*, 43–51.

Piao, S. L., Fang, J. Y., Zhou, L. M., Guo, Q. H., Henderson, M., Ji, W., et al. (2003). Interannual variations of monthly and seasonal normalized difference vegetation index (NDVI) in China from 1982 to 1999. *Journal of Geophysical Research*, *108*(D14), 4401. http://dx.doi.org/10.1029/2002JD002848.

Quiring, S. M., & Ganesh, S. (2010). Evaluating the utility of the Vegetation Condition Index (VCI) for monitoring meteorological drought in Texas. *Agricultural and Forest Meteorology*, *150*, 330–339.

Rhee, J., Im, J., & Carbone, G. J. (2010). Monitoring agricultural drought for arid and humid regions using multi-sensor remote sensing data. *Remote Sensing of Environment*, *114*, 2875–2887.

Rouault, M., & Richard, Y. (2003). Intensity and spatial extension of drought in South Africa at different time scales. *Water SA*, *29*, 489–500.

Rouse, J. W., Haas, R. H., Schell, J. A., & Deering, D. W. (1973). Monitoring vegetation systems in the great plains with ERTS. *Proceedings of the Third ERTS Symposium. NASA SP-351*, *Vol. 1*. (pp. 309–317)Washington, DC: NASA.

Sheffield, J., & Wood, E. F. (2007). Characteristics of global and regional drought, 1950 – 2000: Analysis of soil moisture data from off-line simulation of the terrestrial hydrologic cycle. *Journal of Geophysical Research*, *112*, D17115. http://dx.doi.org/10.1029/2006JD008288.

Trenberth, K. E., Dai, A., Rasmussen, R. M., & Parsons, D. B. (2003). The changing character of precipitation. *Bulletin of the American Meteorological Society*, *84*, 1205–1217.

Trenberth, K. E., Overpeck, J. T., & Solomon, S. (2004). Exploring drought and its implications for the future. *EOS. Transactions of the American Geophysical Union*, *85*. http://dx.doi.org/10.1029/2004EO030004.

Vicente-Serrano, S. M. (2007). Evaluating the impact of drought using remote sensing in a Mediterranean, semi-arid region. *Natural Hazards*, *40*, 173–208.

Wagner, W., Lemoine, G., & Rott, H. (1999). A method for estimating soil moisture from ERS scatterometer and soil data. *Remote Sensing of Environment*, *70*, 191–207.

Wan, Z., Wang, P., & Li, X. (2004). Using MODIS land surface temperature and normalized difference vegetation index products for monitoring drought in the southern Great Plains, USA. *International Journal of Remote Sensing*, *25*, 61–72.

Wang, H. J. (2001). The weakening of the Asian monsoon circulation after the end of 1970's. *Advances in Atmospheric Sciences*, *18*, 376–386.

Wang, B., & Ho, L. (2002). Rainy season of the Asian-Pacific summer monsoon. *Journal of Climate*, *5*, 386–398.

Wang, A. H., Lettenmaier, D. P., & Sheffield, J. (2011). Soil moisture drought in China, 1950–2006. *Journal of Climate*, *24*, 3257–3271.

Wang, L., & Qu, J. J. (2007). NMDI: A normalized multi-band drought index for monitoring soil and vegetation moisture with satellite remote sensing. *Geophysical Research Letters*, *34*. http://dx.doi.org/10.1029/2007GL031021.

Wetherald, R. T., & Manabe, S. (1999). Detectability of summer dryness caused by greenhouse warming. *Climatic Change*, *43*, 495–511.

Wetherald, R. T., & Manabe, S. (2002). Simulation of hydrologic changes associated with global warming. *Journal of Geophysical Research*, *107*(D19), 4379. http://dx.doi.org/10.1029/2001JD001195.

Wilhite, D. A. (2000). Drought as a natural hazard: Concepts and definitions. In D. A. Wilhite (Ed.), *Drought. A Global Assessment*, *Vol. I*. (pp. 3–18)London: Routledge.

Wilhite, D. A. (2005). Drought as hazard: Understanding the natural and social context. In D. A. Wilhite (Ed.), *Drought and Water Crisis: Science, Technology, and Management Issues* (pp. 5–10). Boca Raton: Taylor and Francis Group.

WMO (2006). Drought monitoring and early warning: Concepts, progress and future challenges. *World Meteorological Organization, Report WMO-No. 100*692-63-11006-9 (24 pp.).

Zhang, A. Z., Jia, G. S., Wang, H. S., & Zhao, T. B. (2011). Validation of land surface temperature derived from 37-GHz AMSR-E over northern China. *Atmospheric and Oceanic Science Letters*, *4*, 257–263.

Zhang, A. Z., Jia, G. S., Wang, H. S., Zhao, T. B., Feng, J. M., & Ma, Z. G. (2011). Evaluation of AMSR-E derived soil moisture over northern China. *Atmospheric and Oceanic Science Letters*, *4*, 223–228.